Bonding and Electronic Structure of Superconducting NbPS

Douglas A. Keszler† and Roald Hoffmann*

Contribution from the Department of Chemistry and Materials Science Center, Cornell University, Ithaca, New York 14853-1301. *Received May 12, 1986*

Abstract: Tight-binding band structure calculations performed on the structure of niobium phosphide sulfide are analyzed. The bonding of the linear semicontinuous chain of P atoms present in this material is analyzed with a two-dimensional model; a Nb–P interaction that disrupts the σ bonding within the chain leads to the observed P–P distances. A crystal orbital centered on the Nb atoms that is nonbonding with the P and S atoms in segments of the Brillouin zone affords a peak in the density of states at the Fermi level that is correlated with the observed high superconducting transition temperature. The metal-to-metal bonding is examined, and the structures and physical properties of some postulated compounds are anticipated.

Cursory consideration of the formula NbPS[1] might lead one to anticipate for it the simple valence description Nb^{5+}, P^{3-}, S^{2-}. With a metal atom having a d^0 electron configuration and nonmetal atoms having filled valence shells, semiconducting electrical properties would be anticipated. In fact, the compound is metallic, transforming to a superconductor at 12 K, among the higher transition temperatures for a ternary material.[2] These physical properties and certain unusual structural features in this compound have prompted our investigation of its electronic structure.

The crystal structure of NbPS may be considered to be composed of motif **1**, two metal-centered bicapped trigonal prisms sharing a rectangular face. In this motif P atoms are located at the vertices of the rectangular face that is shared by each prism; a short distance, 2.5 Å, between pairs of these P atoms clearly indicates some bonding. The S atoms are positioned at the remaining vertices of the trigonal prism and at the capping sites. Within this environment of P and S atoms is located a Nb dimer, two Nb atoms separated by 2.9 Å.

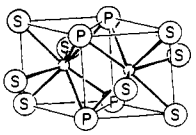

1

This motif occurs in a number of pnictides,[3] thiophosphates,[4] chalcogenides,[5] and chalcogenide halides[6] of transition-metal ions, distorting and associating in a variety of ways to form several unique structural types with diverse physical properties. After detailing some of the characteristics of NbPS, we will return to a consideration of this unit.

The full three-dimensional structure of NbPS that results from assemblage of motif **1** by sharing certain vertices and edges is shown in Figure 1. The units join through S atoms that are positioned at the vertices of trigonal prisms and at the capping sites of adjacent prisms; their tetrahedral coordination by Nb atoms is normal. The motif condenses along the z axis by sharing triangular faces of the prisms, making for separation along z of 3.44 Å between the Nb atoms. This separation, coupled with the short Nb–Nb distance within the motif, results in a chain of interacting Nb dimers having their short bonding axis orthogonal to the translational direction z. This feature may be contrasted to the metal dimers of the structures $NbCl_4$,[7] MoO_2,[8] and marcasite,[9] in which the bonding axes of the metal dimers are collinear with the translational direction.

Along the y axis, the units are tethered by a short P–P contact, 2.2 Å, that is typical of a single bond.[10] This separation, together with that within a prism which we mentioned above, 2.5 Å, affords a linear semicontinuous chain of P atoms extending along the y axis. This chain and the chain of Hg atoms in the compound Hg_3AsF_6 are two of the few reported examples of linear strings of a single main group atom.[11] P atoms certainly exhibit a proclivity toward nonlinear catenation, forming zigzag chains in several compounds. For example, there is an infinite chain having P–P–P angles of 107.1° and 109.2° in the compound PdP_2.[12] Similar zigzag chains are observed in the compounds LaP_2,[13a] α-CeP_2,[14a] GdPS,[14b] $SrSb_2$,[15a] $CaSb_2$,[15b] $SrCuSn_2$, and $BaCuSn_2$.[15c] A general discussion of the formation of such chains by distortion of a square net is given in another paper.[16]

†Present address: Department of Chemistry, Oregon State University, Corvallis, OR.

(1) Donohue, P. C.; Bierstedt, P. E. *Inorg. Chem.* **1969**, *8*, 2690.
(2) See, for example: Shelton, R. N. In *Superconductivity in d- and f-Band Metals*; Buckel, W., Weber, W., Eds.; Kernforschungzentrum: Karlsruhe, 1982; p 123.
(3) (a) Furuseth, S.; Kjekshus, A. *Nature (London)* **1964**, *203*, 512. (b) Hulliger, F. *Nature (London)* **1964**, *204*, 775. (c) Furuseth, S.; Kjekshus, A. *Acta Chem. Scand.* **1964**, *18*, 1180. (d) Brown, A. *Nature (London)* **1965**, *206*, 502. (e) Furuseth, S.; Selte, K.; Kjekshus, A. *Acta Chem. Scand.* **1965**, *19*, 95. (f) Rundqvist, S. *Nature (London)* **1966**, *211*, 847. (g) Jensen, P.; Kjekshus, A.; Skansen, T. *Acta Chem. Scand.* **1966**, *20*, 403. (h) Jeitschko, W.; Donohue, P. C. *Acta Crystallogr.* **1973**, *B29*, 783. (i) Gölin, B.; Carlsson, B.; Rundqvist, S. *Acta Chem. Scand.* **1975**, *A29*, 706. (j) Kanno, R.; Kinomura, N.; Koizumi, M.; Nishigaki, S.; Nakatsu, K. *Acta Crystallogr.* **1980**, *B36*, 2206.
(4) (a) Brec, R.; Ouvrard, G.; Evain, M.; Grenouilleau, P.; Rouxel, J. *J. Solid State Chem.* **1983**, *47*, 174. (b) Fiechter, S.; Kuhs, W. F.; Nitsche, R. *Acta Crystallogr.* **1980**, *B36*, 2217. (c) Evain, M.; Brec, R.; Ouvrard, G.; Rouxel, J. *Mat. Res. Bull.* **1984**, *19*, 41. (d) Evain, M.; Queignec, M.; Brec, R.; Rouxel, J. *J. Solid State Chem.* **1985**, *56*, 148.
(5) (a) Meerschaut, A.; Quēmas, L.; Berger, R.; Rouxel, J. *Acta Crystallogr.* **1979**, *B35*, 1747. (b) Furuseth, S.; Klewe, B. *Acta Chem. Scand.* **1984**, *A38*, 467.
(6) (a) von Schnering, H.-G.; Beckmann, W. *Z. Z. Anorg. Allg. Chem.* **1966**, *347*, 231. (b) Schäfer, H.; Beckmann, W. *Z. Anorg. Allg. Chem.* **1966**, *347*, 225. (c) Rijnsdorp, J.; Jellinek, F. *J. Solid State Chem.* **1978**, *28*, 149. (d) Marcoll, J. D.; Rabenau, A.; Mootz, D.; Wunderlich, M. *Rev. Chim. Miner.* **1974**, *11*, 607.
(7) (a) Cotton, F. A.; Rice, C. E. *Inorg. Chem.* **1977**, *16*, 1865. (b) Whangbo, M.-H.; Foshee, M. J. *Inorg. Chem.* **1981**, *20*, 113. (c) Bullett, D. W. *Ibid.* **1980**, *19*, 1780.
(8) Goodenough, J. B. In *Progress in Solid State Chemistry*; Reiss, H., Ed.; Pergamon: New York, 1971; Vol. 5, p 145.
(9) Brostigen, G.; Kjekshus, A. *Acta Chem. Scand.* **1970**, *24*, 2993.
(10) Maxwell, L. R.; Henricks, S. B.; Mosley, V. M. *J. Chem. Phys.* **1935**, *3*, 699.
(11) (a) Brown, I. D.; Cutforth, B. D.; Davies, C. G.; Gillespie, R. J.; Ireland, P. R.; Vekris, J. E. *Can. J. Chem.* **1974**, *52*, 791. (b) Schultz, A. J.; Williams, J. M.; Miro, N. D.; MacDiarmid, A. G.; Heeger, A. J. *Inorg. Chem.* **1978**, *17*, 646–649. (c) Miro, N. D.; MacDiarmid, A. G.; Heeger, A. J.; Garito, A. F.; Chiang, C. K.; Schultz, A. J.; Williams, J. M. *J. Inorg. Nucl. Chem.* **1978**, *40*, 1351. (d) McCarley and co-workers have recently synthesized $SnMo_4O_6$ containing linear strings of Sn atoms (personal communication).
(12) Zachariasen, W. H. *Acta Crystallogr.* **1963**, *16*, 1253.
(13) (a) von Schnering, H.-G.; Wichelhaus, W.; Schulze Nahrup, M. *Z. Anorg. Allg. Chem.* **1975**, *412*, 193. (b) Hahn, H.; Stocks, K. *Naturwissenschaften* **1968**, *55*, 389.
(14) (a) Hegyi, I. J.; Loebner, E. E.; Poor, E. W., Jr.; White, J. G. *J. Phys. Chem. Solids* **1963**, *24*, 333. (b) Hulliger, F.; Schmelczer, R.; Schwarzenbach, D. *J. Solid State Chem.* **1977**, *21*, 371.
(15) (a) Deller, K.; Eisenmann, B. *Z. Naturforsch.* **1976**, *31b*, 1146. (b) Deller, K.; Eisenmann, B. *Z. Anorg. Allgem. Chem.* **1976**, *425*, 104. (c) May, N.; Schäfer, H. *Z. Naturforsch.* **1974**, *29b*, 20.

0002-7863/87/1509-0118$01.50/0

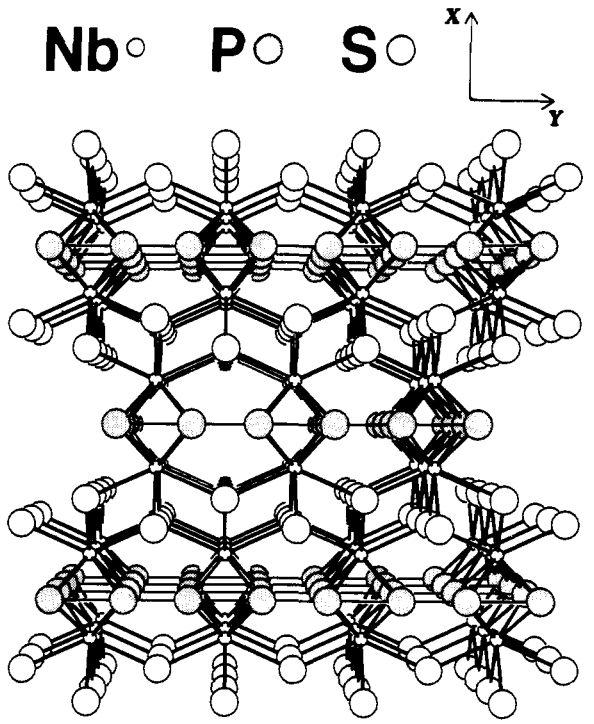

Figure 1. Structure of NbPS viewed along the z axis.

Why, in the P string of NbPS, do the distances alternate as they do, and how does this distortion relate to the very important electrical properties? To begin the analysis of these features we will do some electron counting. First, for the P chain, if the longer intraprism P–P distance is disregarded as a bonding interaction, a broken chain, **2**, consisting of dimers of composition P_2^{4-} results. A continuous chain of P atoms, **3**, with a single bond between each atom and six valence electrons per site affords the representation $(P_n)^{n-}$ or P^{1-}. As there are no P–S or S–S distances indicative of bonding, the S atoms are counted as sulfide S^{2-}. We can now derive the valence descriptions Nb^{4+}, P^{2-}, S^{2-} assuming chain **2** and Nb^{3+}, P^{1-}, S^{2-} assuming chain **3**. In fact, since all the distances in the P chain are indicative of some bonding, its valence description lies somewhere between **2** and **3**, meaning the formal valence state of the Nb atoms is somewhere between Nb^{4+} and Nb^{3+}. To go from **2** to **3** the chain must be oxidized and the metal

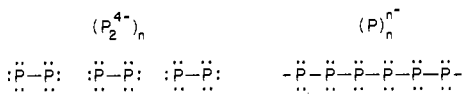

2 **3**

atoms reduced. For this to occur, as it partly does in the three-dimensional structure, there must be a crystal orbital on the Nb atoms at an energy low enough to accept electrons from the P chain. It will be seen that this orbital is present and is a consequence of translational symmetry. Before examining the nature of this orbital and the band structure of NbPS, we will discuss the distances observed in the P chain.

P–P Bonding

To model the bonding in the P chain we use two slabs derived from the three-dimensional structure. **4** is a two-dimensional raft with P atoms equally spaced at 2.36 Å along the y axis and 3.44 Å along the z axis. **5** obtains from **4** by capping each rectangular hollow along z and alternate hollows along y, above and below with Nb atoms bonded to S atoms. This slab is a two-dimensional model of the full structure; the two types of P–P interactions along y, which we call intraprism and interprism, should be apparent. The coordination number of the Nb atoms is reduced from eight in the observed structure to six in our model by scission of S atoms

(16) (a) Tremel, W.; Hoffmann, R. *J. Am. Chem. Soc.*, following paper in this issue. (b) Jeitschko, W. *Acta Cyrstallogr.* **1974**, *B30*, 2565.

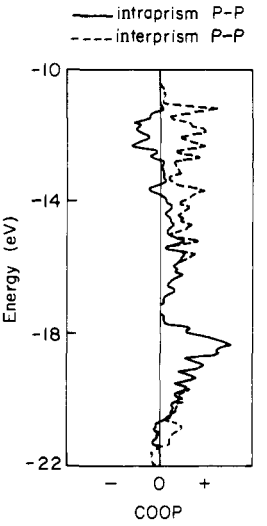

Figure 2. Crystal orbital overlap populations for intraprism P–P bonding (—) and interprism P–P bonding (---) in raft **5**.

from their capping positions. This reduction in coordination number does not much affect the applicability of the nature of the P–P and Nb–P bonding in the model to that of the full structure.

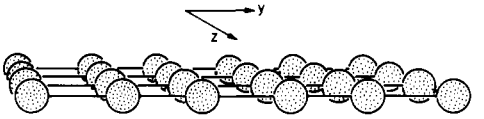

4

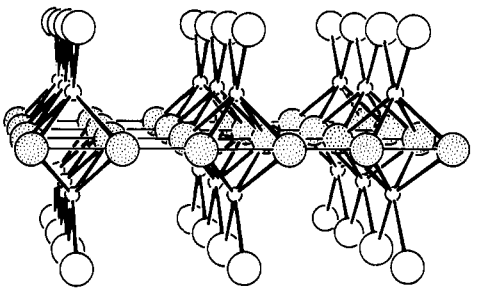

5

Before proceeding, we should ascertain that **5** exhibits bonding features consistent with the observed structure. After this, we may proceed to an analysis of some of its details. The overlap populations for the intraprism and interprism P–P interactions, computed at *equal* P–P separation, are 0.26 and 0.53, respectively. The trend indicated by those overlap populations is in agreement with the structure; the smaller population corresponds to the longer distance in the observed structure. A convenient graphical method for displaying these populations is provided by the COOP curves shown in Figure 2, the density of states weighted by the overlap populations of the P–P bonds. In these curves the P–P bonding character is plotted as a function of energy from the overlap populations of a representative sampling of all the states in a selected energy interval. The curve has positive (bonding) and negative (antibonding) regions, and its integration up to the Fermi level affords the total overlap population. We see that the two types of P–P interactions are similar up to −16 eV, at which point the interprism population begins to exhibit greater bonding character. Around −12 eV the intraprism overlap population is actually negative. The Fermi level for this slab rests just below −10 eV.

We have a system that correctly models the P–P distances; a lengthening of the intraprism P–P distance is anticipated. From

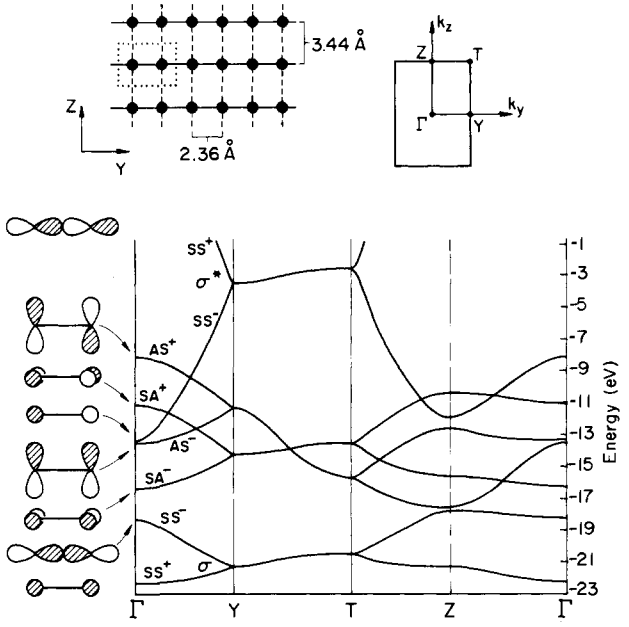

Figure 3. Band structure for the two-dimensional P array **4**, drawn in the *yz* plane at upper left.

a molecular viewpoint, how might we account for this result? We can easily extract (on paper) fragment **6** from model **5**. And this fragment is isoelectronic to fragment **7** containing two acetylenes.

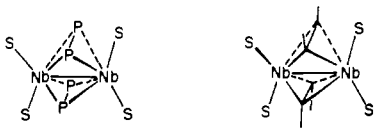

6

7

Such perpendicular acetylene complexes are well-known,[17] and their bonding characteristics have been studied.[18] Nonligated C_2H_2 has a C–C bond length of 1.21 Å while the bridged acetylene ligands in complexes of the type **7** exhibit a lengthening of the C–C bond to 1.3–1.4 Å. The Dewar–Chatt–Duncanson model[19] provides a useful explanation for this lengthening of the C–C bond, and it does so in discrete P_2 complexes of type **6**. But our solid-state structures are inherently delocalized, and for an understanding of intra- and intermolecular P–P bonding we must begin from another starting point.

The band structure for array **4** is shown in Figure 3. In anticipation of the formation of **5**, the unit cell is chosen to contain two P atoms, twice the primitive cell. The intracellular P–P contact in **4** corresponds to the intraprism contact of **5**, and likewise the intercellular contact of **4** corresponds to the interprism contact of **5**. The bands along the line Γ–Y are labeled as S or A, symmetric or antisymmetric with respect to $\sigma(yz)$ or $\sigma(xy)$, and "+" or "−", symmetric or antisymmetric with respect to the screw axis. By symmetry the P–P interactions along this line are separated into σ and π types.

It is not difficult to understand the origins of this band structure. The spacing of the P chains along *z* is a somewhat distant 3.44 Å. The bands have relatively small dispersions along the ΓZ line. A construction of the band structure from that of a one-dimensional P_n chain, **8**, is suggested.

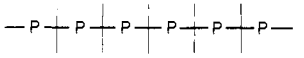

8

The π and π^* orbitals of such a chain will give a classical free-electron-type band. Burdett has described the σ bonding in such a linear chain of atoms.[20] With one atom per unit cell, the band structure derived from the σ orbitals is given in **9**. There is a band crossing toward the zone boundary, inverting the s and p character. Substantial mixing, enhanced by a smaller s,p orbital splitting, takes place. The net result is a lower band that is bonding throughout the zone and a higher band that is antibonding.

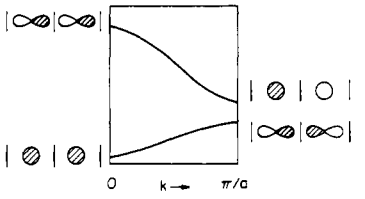

9

Next we double the one-dimensional primitive cell, in preparation for building up the raft. This has as a trivial consequence the "folding back" indicated in **10**. A similar folding back takes place for the π bands, not indicated here.

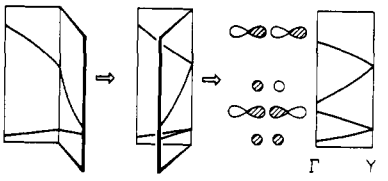

10

We have almost reached the band structure of the raft along ΓY, as inspection of that line in Figure 3 shows. All that remains is to note that in the two-dimensional material the π_x and π_z bands are no longer degenerate and that at Γ π_z is above π_x because there is a weak σ antibonding component in the π_z crystal orbital, **11a** vs. **11b**.

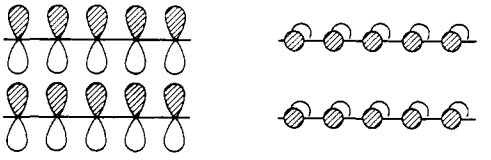

11

If we have six electrons per P atom, the Fermi level for the slab is at −11 eV. A portion of the σ^* band is filled and a portion of the AS^+ band (π^*) remains empty. The bonding in the slab is thus characterized by sp σ bonding with a small contribution of π bonding. In this state our raft would be a metallic conductor, with a distortion via a Peierls-type mechanism[21] expected only for a lengthening of the cell parameter *y* so as to form, for example, weakly interacting P_2^{2-} units.

Now we interact this two-dimensional raft with the Nb atoms to form **5**. A breakdown of the inter- and intraprism P–P bonding in the final lattice indicates that the difference in P–P bonding derives mainly from the σ rather than the π orbitals of the chain (note the difference from what would happen in a molecular P_2 complex). So we will concentrate on the σ bands, especially on

(17) See, for example: (a) Cotton, F. A.; Jamerson, J. D.; Stults, B. R. *J. Am. Chem. Soc.* **1976**, *98*, 1774. (b) Green, M.; Grove, D. M.; Howard, J. A. K.; Spencer, J. L.; Stone, F. G. A. *J. Chem. Soc., Chem. Commun.* **1976**, 759. (c) Freeland, B. H.; Hux, J. E.; Payne, N. C.; Tyers, K. G. *Inorg. Chem.* **1980**, *19*, 693. (d) Jack, T. R.; May, C. J.; Powell, J. *J. Am. Chem. Soc.* **1977**, *99*, 4704.

(18) Hoffman, D. M.; Hoffmann, R.; Fisel, C. R. *J. Am. Chem. Soc.* **1982**, *104*, 3858.

(19) (a) Dewar, M. J. S. *Bull. Soc. Chim. Fr.* **1951**, *18*, C71–C79. (b) Chatt, J.; Duncanson, L. A. *J. Am. Chem. Soc.* **1953**, *75*, 2939.

(20) Burdett, J. K. *Prog. Solid State Chem.* **1984**, *15*, 173.

(21) Peierls, R. E. *Quantum Theory of Solids*; Oxford University Press: London, 1955; p 108.

those formed from p_σ which are better matched in energy with the Nb d block.

12 indicates schematically where the Nb d band falls relative to the crucial p_σ ($SS^- - SS^+$) band. Because of a mismatch in energy, there is little interaction between the Nb and P bands at T. Interaction becomes favorable toward Y, where this mismatch

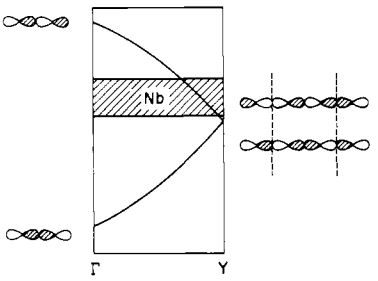

12

is reduced. The strength of this interaction is reflected in the partitioning of the intraprism and interprism overlap populations along the line Γ–Y; they are equal at Γ and disparate at Y. We should concentrate on the interactions at symmetry point Y.

On the right side of **12** are shown the degenerate bands of point Y. The dashed lines in this structure represent the symmetry planes for the intraprism P–P interactions. For the *y* band, one combination is symmetric with respect to this plane whereas the other is antisymmetric. Each of these combinations will select their symmetry partner from the Nb d levels. Four of these Nb–P interactions, two at the symmetry point Y and two at the point T, are shown in **13** with the values of their overlap integrals. The

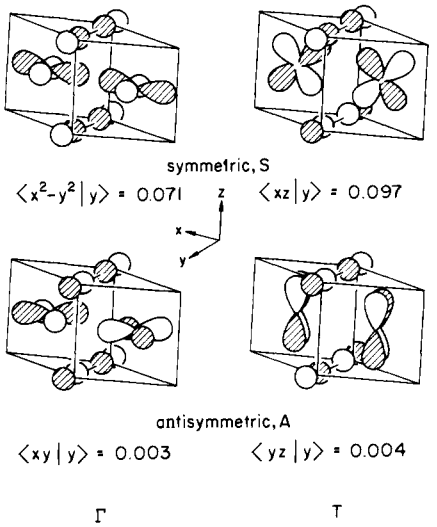

13

values derived from Nb orbitals interacting with the symmetric combination are more than an order of magnitude greater than the corresponding interactions with the antisymmetric combination; the lobes of the Nb orbitals are directed toward the lobes of the *y* orbitals for the symmetric combination and toward the nodes for the antisymmetric combination. Hence, the interaction of Nb levels and the symmetric combination of P levels affords a strong multicenter bond; the symmetric Nb levels are better electron acceptors than their antisymmetric counterparts. The magnitudes of the overlap integrals for the Nb p and s orbitals interacting with the P levels follow the same trend, further increasing through hybridization the ability of the symmetric Nb orbitals to accept electrons. Consequently, the symmetric combinations afford weakened P–P intraprism bonding and simultaneously, as seen by consideration of the bands shown in Figure 3, weakened interprism antibonding. There is only a small Nb–P interaction for the antisymmetric combination, hence little change in the P–P intraprism antibonding and interprism bonding occurs. It is these P–P interactions that dominate the COOP curve above −14 eV in Figure 2. The symmetric combinations are split about the Fermi level by their stronger Nb–P interaction. The net effect is a weakening of the intraprism P–P bond and a slight strengthening of the interprism bond, resulting from a selective transfer of P–P σ bonding into Nb–P bonding.

Band Structure of NbPS

Near the Fermi level, the bands of NbPS should mostly be of Nb d-orbital character. The detailed nature of these bands is determined by the local crystal field, metal-to-metal bonding, and translational symmetry. To see the effects of each of these components we will consider an interaction diagram for fundamental unit **1** and then add to it translational symmetry.

The local coordination environment of each Nb atom in motif **1** is a bicapped trigonal prism. This eight-coordinate environment affords a crystal-field splitting of one d orbital below four.[22] As shown in **14**, interaction of two of these prisms through a common quadrilateral face to form **1** yields a pattern of one d orbital below nine, a result of metal-to-metal bonding; the lowest a_g orbital is metal-to-metal σ bonding. The next orbital up, b_{3u}, is chiefly d_{z^2} and δ^* in character.

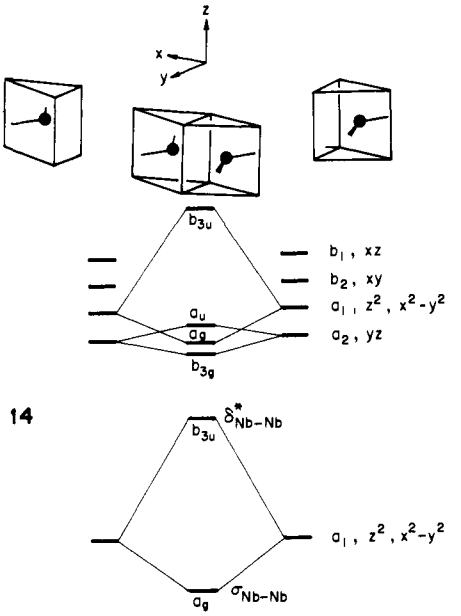

From this diagram we would anticipate occupation of the level a_g, formation of a metal-to-metal σ bond, and diamagnetic behavior for a molecular or extended solid-state compound formed from isolated units with geometry **1** having a metal atom with a formal d^1 configuration. There exists a set of compounds in which these units are isolated, linked only by non-metal bridges; this set includes the compounds NbS_2Cl_2,[6] $Nb_3Se_5Cl_7$,[6] Nb_2Se_9,[5] and MoS_2Cl_3.[6] Each compound formally has a d^1 metal atom and each is a diamagnetic semiconductor with a band gap of >1.2 eV corresponding to the separation between the lowest level, a_g, and level b_{3u} in **14**. This description is consistent with the results of calculations performed by Bullett.[23]

How may we apply this local description to NbPS? From our electron counting we determined that there is more than one valence electron for each Nb atom, implying locally occupation of the high-lying level b_{3u}. Since the S atoms are present as sulfide S^{2-}, the electrons proposed to occupy the level b_{3u} must come from the P atoms, but this level is more than 1 eV above a_g. How do P atoms, which are themselves oxidants, surmount this 1-eV barrier and donate electrons to the Nb atoms? In other words, why is there a chain of P atoms rather than discrete P_2^{4-} units present in this structure?

(22) Burdett, J. K.; Hoffmann, R.; Fay, R. C. *Inorg. Chem.* **1978**, *17*, 2553.
(23) Bullett, D. W. *J. Phys. Chem.* **1980**, *13*, 1267.

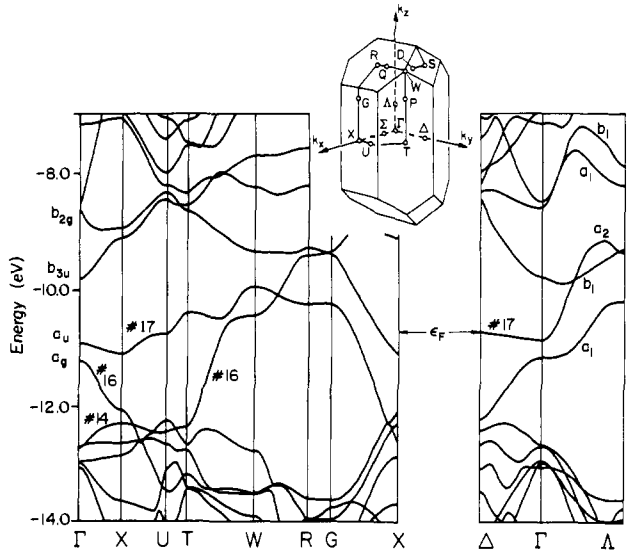

Figure 4. Band structure of three-dimensional NbPS.

The answers to these questions lie in the band structure of NbPS shown in Figure 4. Above −12 eV the bands are mostly of Nb character, and below they have P and S character. As expected from the structure (cf. Figure 1), the greatest dispersion of the Nb-centered bands is along the z axis, the lines T–W, G–X, and Γ–Λ. We can compare the nature of the bands at Γ with the energy levels of **14**. On the left side of the band diagram of Figure 4, four bands have been labeled according to the point group symmetry D_{2h} at Γ, the point group of motifs **1** and **14**. In ascending order these crystal orbitals are labeled a_g, a_u, b_{3u}, and b_{2g}. The lowest of these orbitals, #16, is mostly centered on the S atoms at Γ but it undergoes an avoided crossing along the line Γ–Λ with band #14 which is metal-to-metal σ bonding. These bands thus correspond to the lowest a_g level of **14**. Band #18, b_{3u}, is metal-to-metal δ^* in character and corresponds to the level b_{3u} in our local picture. Between these bands is level #17, labeled a_u. This orbital is at a much lower energy than would have been anticipated from crystal-field arguments. We may determine the nature of this band and provide further comparisons between the bands of the solid and the levels of **14** by inspecting projections of the density of states.

These curves are given in Figure 5 for the Nb-centered d_{z^2}, $d_{x^2-y^2}$, and d_{yz} orbitals. As expected from crystal-field arguments, the d_{z^2} level is weakly split about the Fermi level, with most of the d_{z^2} character resting just above this point. Likewise, as anticipated there is a strong splitting of the $d_{x^2-y^2}$ orbitals with a considerable contribution well above the Fermi level. The d_{yz} orbital is similarly split, but it provides a sizable contribution to the total density of states at the Fermi level. This contribution corresponds to band #17, a_u, in Figure 4.

The nature of this Nb d_{yz} band at Γ is shown in Figure 6. It is characterized as metal-to-metal δ^* within a dimer and antibonding along the translational direction z. This crystal orbital is centered only on the Nb atoms and is nonbonding with respect to the P and S atoms at Γ and along the lines Γ–Δ and Γ–X, a result dictated by *translational* symmetry. Along the line X–U d_{yz} mixes with d_{xz} and along the line U–T it mixes with S orbitals, crossing the Fermi level to afford three-dimensional character to the physical properties.

Now we can associate this band with the metrical details of the P chain and the physical properties of the material. When disrupted by Nb–P bonding, why does the intraprism P–P interaction not lengthen to a nonbonded distance to make discrete P_2^{4-} units? The answer derives in part from the presence of the low-lying d_{yz} band. It acts as a sink for electrons during the oxidation process $P_2^{4-} \rightarrow 2P^{1-} + 2e^-$, a process favored entropically through delocalization of electron density in the Nb d band and by enthalpy in formation of the partial P–P intraprism bond. The other effect that determines this distance arises from the matrix. The distance is to a certain degree dictated by the packing associated with the S atoms which must satisfy their bonding demands on the Nb atoms. Evidence for this view derives from metrical data on the compound NbPSe. In this compound the interprism P–P distance is equal to that in the sulfide whereas the intraprism distance is longer, reflecting the larger size of the Se atom.

The presence of this band may also be correlated to the high superconducting transition temperature. The transition temperature of a superconductor may be approximated as

$$T_c \simeq e^{-1/N_F}$$

where N_F is the density of states at the Fermi level.[24] The d_{yz}

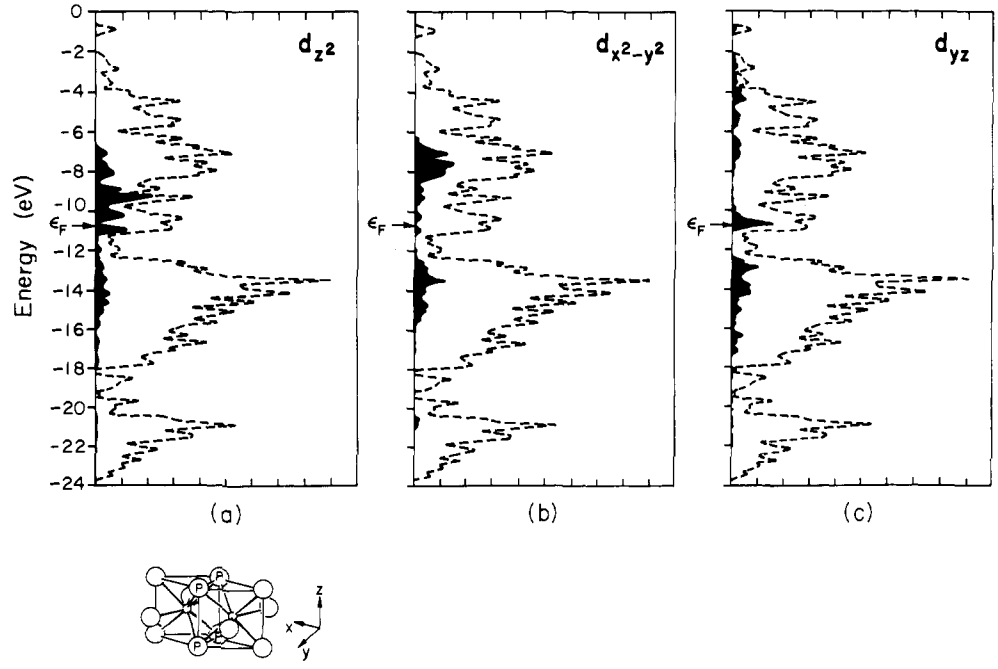

Figure 5. Total density of states (---) for NbPS and the contributions to it of certain Nb atomic orbitals: (a) d_{z^2}, (b) $d_{x^2-y^2}$, (c) d_{yz}. The Fermi level shown is for 17 valence electrons.

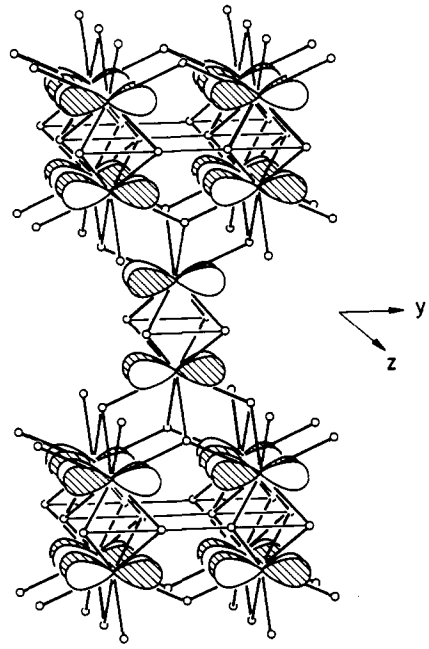

Figure 6. Nb d_{yz} crystal orbital at Γ. The P and S atoms are designated as small circles. A line joins the atoms of the P chain.

band is flat in a large portion of the Brillouin zone, affording a peak in the density of states at the Fermi level (Figure 5c). Now, if we correlate the presence of this peak to the high T_c we expect to observe a singularity in superconducting behavior for an ordered material with this geometry and electron count.

It does not follow, however, that NbPSe, TaPS, and TaPSe will be superconducting. In NbPS a fine balance of the metal–metal, non-metal–non-metal, and metal–non-metal interactions has been attained that places the Fermi level at a peak in the density of states chiefly associated with the d_{yz} crystal orbital. If this balance is perturbed, that is, if the sum of these interactions does not scale linearly and in the same direction for other compounds, the Fermi level will be displaced from this peak in the density of states, to afford compounds that are not superconducting.

From a graph of the projected density of states for the compound NbPSe, we observe the d_{yz} band below the Fermi level. Again, in those portions of the zone where the d_{yz} band is flat, it is metal-to-metal antibonding along the z axis. Because of the larger size of the Se atom, the metal–metal distance along this direction increases from NbPS to NbPSe, affording a reduction of the antibonding interaction that causes the d_{yz} band to fall in energy (#17 in Figure 4). In contraposition, other bands near the Fermi level will rise in energy in the selenide compared with the sulfide; band #16 in Figure 4 is one example. At Γ this band of p_z orbitals is antibonding among the chalcogen atoms. The greater radial extension of the Se p orbitals is not fully compensated by the larger Se···Se distances, causing this crystal orbital to rise in energy. Interactions are scaling inversely; band #16 is emptied of electrons in portions of the zone, with band #17 becoming filled.

We have not performed a calculation on TaPS, but here too we expect the critical d_{yz} band to lie below the Fermi level. The unit cell parameters reported for TaPS[2] differ from NbPS by less than 1%, implying that we can use the refined metrical data of NbPS for our consideration of superconductivity in TaPS. The radial extension of the d orbitals increases from NbPS to TaPS. The flat d_{yz} band, #17, of TaPS should rise in energy with respect to that of NbPS, and some of the remaining metal-centered bands should exhibit a much larger dispersion. The cumulation of the effects should push the d_{yz} band below the Fermi level. As an

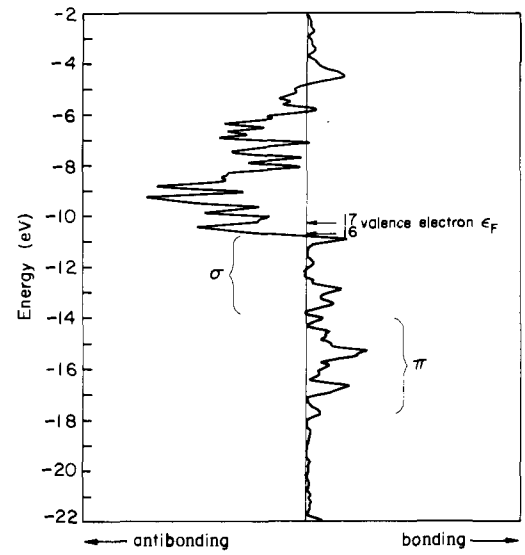

Figure 7. Crystal orbital overlap population curve for Nb–Nb bonding within a dimer unit.

example, we can consider the line Γ–Λ in Figure 4. As noted earlier, the lower a_1 band is mostly centered on the S atoms; its energetic position will change little from NbPS to TaPS. Toward Λ it becomes metal-centered, mostly d_{z^2}; at Λ it is metal–sulfur antibonding and metal–metal antibonding along the chain direction. Hence, relative to NbPS, this orbital should lie at a considerably higher energy at Λ. The a_1 band has a greater dispersion in TaPS, a dispersion that should be large enough to permit a greater portion of it to rise above the flat d_{yz} band. The d_{yz} band rises as a consequence of a stronger metal–metal interaction only, whereas the dispersion of the a_1 band arises from both stronger metal–metal and metal–sulfur interactions.

This argument can be extended to other lines, for example, T–W and G–X; the result should be a lowering of the d_{yz} band beiow the Fermi level. Superconductivity has not been observed in the compounds NbPSe, TaPS, and TaPSe, at least by measurements down to 2.0 K.[1]

These compounds with the structural type NbPS, certain lanthanide compounds forming with the structural type GdPS,[16] and the compound PdPS[16b] are the only reported examples of compounds that may be classified as transition-metal phosphide chalcogenides. Many additional examples of such materials probably remain to be synthesized. From our results on NbPS, we suggest the preparation of the compounds MoPS and NbPBr with 17 valence electrons. If these materials form with the NbPS structure, we anticipate from a rigid-band model that the Fermi level would locate near a peak in the total density of states just below −10 eV (cf. Figure 5). A slight lengthening of the metal–metal distance within the dimer units is also anticipated in these materials. This result derives from consideration of the COOP curve shown in Figure 7. The bonding is characterized by mostly π interactions below σ interactions. This inverted ordering has been discussed elsewhere,[25] resulting from through-bond coupling with the P atoms. In a compound with 17 valence electrons, metal-to-metal antibonding bands become occupied, which should lead to a longer metal–metal distance.

To probe the nature and effects of the nonbonding d_{yz} band, a set of compounds should be synthesized in which the electron concentration could be varied to place this band at the Fermi level. This band will be present in any material in which the two-dimensional slab **5** of D_{2h} symmetry is present. Preparation of compounds such as Cu_xZrPBr and Cu_xZrPS in which the Cu concentration could be varied to alter the electron count and position of the Fermi level appears especially interesting. Indeed,

(24) This statement is oversimplified. See: McMillan, W. L. *Phys. Rev.* **1968**, *167*, 331.

(25) Shaik, S.; Hoffmann, R.; Fisel, C. R.; Summerville, R. H. *J. Am. Chem. Soc.* **1980**, *102*, 4555.

Table I. Parameters Used in Extended-Hückel Calculations

	orbital	H_{ii}, eV	l	2	C_1[a]	C_2[a]
Nb	4d	-12.10	4.08	1.637	0.6404	0.5519
	5s	-10.10	1.89			
	5p	-6.86	1.85			
P	3s	-18.60	1.88			
	3p	-14.00	1.63			
S	3s	-20.00	2.12			
	3p	-13.30	1.83			

[a] Coefficients of the double-ζ expansion.

these and related syntheses are currently under investigation.

Acknowledgment. Douglas Keszler thanks J. Silvestre, C. Zheng, and R. Wheeler for helpful discussions. We are also grateful to three reviewers for a careful reading of the paper, pointing out several errors and omissions. Our work was generously supported by the National Science Foundation through Research Grants DM 8217722 to the Materials Science Center at Cornell University and Grant CHE 8406119.

Appendix

All calculations were performed with the extended Hückel method.[26] The parameters used for the Nb, P, and S orbitals are listed in Table I. A set of 28 or more k points was chosen to calculate average properties.[27]

Registry No. NbPS, 26153-57-1; NbPSe, 26134-84-9; TaPS, 26134-85-0; TaPSe, 104911-45-7.

(26) Hoffmann, R. *J. Chem. Phys.* **1963**, *39*, 1397.
(27) Pack, J. D.; Monkhorst, J. *Phys. Rev. B* **1977**, *16*, 1748.

Square Nets of Main Group Elements in Solid-State Materials

Wolfgang Tremel[1] and Roald Hoffmann*

Contribution from the Department of Chemistry and Materials Science Center, Cornell University, Ithaca, New York 14853. *Received May 29, 1986*

Abstract: The Cu_2Sb/ZrSiS/PbFCl structure type—ubiquitous, as the number of synonyms shows—may be derived conceptually from a layering of square nets of atoms. One group of phases can be described as MAB (M: large metal atom; A and B: main group elements). M and B atoms form associated square nets. They are separated by a 4^4 layer of A atoms which is twice as dense as the individual M and B layers. In the more covalent, metallic MAB phases the A···A contacts within the 4^4 layers—which are our prime focus of interest—indicate bonds of fractional order. For M = Ln, A = P, As, and B = S two sets of distorted structure types exist. In the GdPS and CeAsS structures the layers distort to form cis–trans poly-P or zigzag poly-As chains, respectively. The electronic structure of the MAB phases is constructed, and the distortion is traced to a band crossing at the Fermi level. The deformation—a second-order Jahn–Teller distortion in the solid state—is driven by the formation of an energy gap at the Fermi level. The relative electronegativity of the M and A atoms dictates whether the distorted or undistorted structure is preferred. A prerequisite for the distortion to occur is a separation of valence band and metal d block. The general distortion type square net → zigzag chain can also be found in other phases containing 4^4 nets of main group atoms. Further examples treated here are the distortion from the $ZrSi_2$ to the $CaSb_2$ type structures and a deformation type found in ATB_2 phases, exemplified by $SrZnBi_2$.

It is not easy to think about extended structures in the solid state. There is always arbitrariness in the description of crystal structures, because one may want to stress either the chemistry of physical properties of a material or emphasize the structural relationship to other compounds. Choices of vantage must be made. Taking "Schnering's spectacles" and discovering clusters in solid-state compounds[2] is one particularly nice way to visualize crystal structures. Another, more traditional concept in crystal chemistry describes structures in terms of coordination polyhedra.[3] These polyhedra may then be oriented in various ways and connected via corners, edges, or faces. An alternative approach considers structures as being built up from two-dimensional layer stackings. The resulting description based on closest packing is especially useful in cases where polyhedra are difficult to define. Still another concept describes crystal structures in terms of stacked layers, but focussing now on the atom connectivity. Many structure types can be covered by considering only square (4^4), triangular (3^6), hexagonal (6^3), or kagome (3636) networks, **1a–d**.[4]

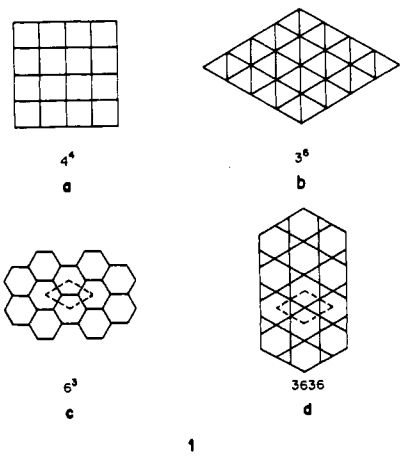

1

Each description may be mathematically well-defined but need not have a prior claim to general chemical or physical validity. A pragmatic perspective is best. To obtain a convenient description of solids we often switch from one description to another, according

(1) DAAD/NATO Postdoctoral Fellow 1984–1985. DFG Fellow 1985–1986. Present addresss: Anorganisch-Chemisches Institut der Universität, Correnstr. 36, D4400 Münster, F.R.G.
(2) (a) von Schnering, H.-G. *Angew. Chem.* **1983**, *93*, 44; *Angew. Chem., Int. Ed. Engl.* **1981**, *20*, 33. (b) Simon, A. *Angew. Chem.* **1981**, *93*, 23; *Angew. Chem., Int. Ed. Engl.* **1981**, *20*, 1.
(3) Gladyshevskii, E. I.; Grin', Yu. N. *Kristallografiya* **1981**, *26*, 1204; *Sov. Phys. Crystallogr.* **1981**, *26*, 683.
(4) (a) Pearson, W. B. *The Crystal Chemistry and Physics of Metals of Alloys*; Wiley: Interscience, 1972. (b) O'Keeffe, M.; Hyde, B. G. *Philos. Mag.* **1980**, *295A*, 38.
(5) (a) von Fedorov, E. *Z. Kristallogr. Mineral.* **1904**, *38*, 321. (b) von Fedorov, E. *Das Krystallreich, Tabellen zur krystallchemischen Analyse*, Petrograd, 1920.
(6) (a) Laves, F. *Theory of Alloy Phases*; Cleveland, Ohio, 1956; pp 124. (b) Laves, F. *Phase Stability in Metals and Alloys*; McGraw-Hill: New York, 1967; p 85.

0002-7863/87/1509-0124$01.50/0